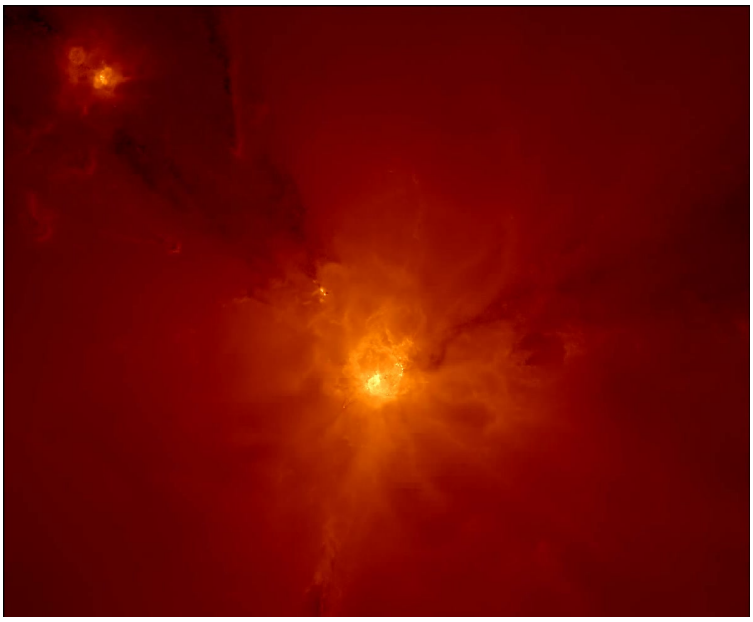

Lyman-α Radiative Transfer

Aaron Smith*

I. INTRODUCTION

The Lyman-α (Lyα) line of neutral hydrogen (H I) is an important probe of galaxy formation and evolution throughout cosmic history [16]. However, due to the complex nature of resonant scattering of Lyα photons in optically-thick environments, the necessary radiative transfer modeling and interpretation of observations are often challenging [6]. Encouragingly, the fundamental physical processes are well studied and a few analytic solutions exist in the literature for idealized cases [7, 8, 12, 14]. Furthermore, the development of Monte Carlo radiative transfer (MCRT) codes with acceleration schemes has allowed for an accurate, universal approach to Lyα calculations [e.g. 3, 4, 23]. The MCRT method is commonly used to analyze 3D hydrodynamical simulations in post-processing and explore parameter spaces in empirical modeling. In these notes we provide brief introductions to different MCRT-based methods for Lyα radiative transfer. The primary goal is a high-level understanding of the underlying physics through numerical thought experiments. Although the accompanying codes are not practical for research applications, they are reasonably efficient while still giving "correct" results and transparent enough to provide intuition about unique aspects of Lyα MCRT. In Section II, we introduce the radiative transfer equation, discuss properties of frequency redistribution, and derive an analytic solution for the case of an isothermal uniform slab. In Section III, we present a simplified version of the standard MCRT solution. In Section IV, we provide an alternative approach based on discrete diffusion techniques.

* arsmith@mit.edu

II. RADIATIVE TRANSFER EQUATION

The specific intensity $I_\nu(\boldsymbol{r}, \boldsymbol{n}, t)$ encodes all information about the radiation field taking into account the frequency ν, spatial position $\boldsymbol{r}$, propagation direction unit vector $\boldsymbol{n}$, and time t. The general Lyα radiative transfer equation is given by

$$\frac{1}{c}\frac{\partial I_\nu}{\partial t} + \boldsymbol{n}\cdot\boldsymbol{\nabla} I_\nu = j_\nu - k_\nu I_\nu + \iint k_{\nu'} I_{\nu'} R_{\nu',\boldsymbol{n}'\to\nu,\boldsymbol{n}} \mathrm{d}\Omega' \mathrm{d}\nu' \,, \tag{1}$$

where k_ν is the absorption coefficient, j_ν is the emission coefficient, and the last term accounts for frequency redistribution after partially coherent scattering [6]. The redistribution function R is the differential probability per unit initial photon frequency ν' and per unit initial directional solid angle Ω' that the scattering of such a photon traveling in direction $\boldsymbol{n}'$ would place the scattered photon at frequency ν and directional unit vector $\boldsymbol{n}$ [for the historical development see 9, 21, 22].

It is convenient to convert to the dimensionless frequency

$$x \equiv \frac{\nu - \nu_0}{\Delta\nu_\mathrm{D}} \,, \tag{2}$$

where $\nu_0 = 2.466\times10^{15}$ Hz is the frequency of the Lyα transition, $\Delta\nu_\mathrm{D} \equiv (v_\mathrm{th}/c)\nu_0$ is the Doppler width of the profile, and the thermal velocity in terms of $T_4 \equiv T/(10^4\,\mathrm{K})$ is $v_\mathrm{th} \equiv (2\,k_\mathrm{B}T/m_\mathrm{H})^{1/2} = 12.85\,T_4^{1/2}\,\mathrm{km\,s^{-1}}$. Furthermore, the natural Lyα line width is $\Delta\nu_\mathrm{L} = 9.936\times10^7$ Hz and the 'damping parameter', $a \equiv \Delta\nu_\mathrm{L}/2\Delta\nu_\mathrm{D} = 4.702\times10^{-4}\,T_4^{-1/2}$, represents the relative broadening of the natural line. The frequency dependence of the absorption coefficient is given by the Voigt profile ϕ_Voigt. For convenience we define the Hjerting-Voigt function $H(a,x) = \sqrt{\pi}\Delta\nu_\mathrm{D}\phi_\mathrm{Voigt}(\nu)$ as the dimensionless convolution of Lorentzian and Maxwellian distributions,

$$H(a,x) = \frac{a}{\pi}\int_{-\infty}^{\infty} \frac{e^{-y^2}\mathrm{d}y}{a^2+(y-x)^2} \approx \begin{cases} e^{-x^2} & \text{'core'} \\ \dfrac{a}{\sqrt{\pi}x^2} & \text{'wing'} \end{cases} . \tag{3}$$

The approximate frequency marking the crossover from core to wing is denoted by x_cw, i.e. where $\exp(-x_\mathrm{cw}^2) \simeq a/\sqrt{\pi}x_\mathrm{cw}^2$.

Expressions for the redistribution function and discussions of its properties may be found in [10, 11, 15, 21]. One notational simplification is that the scattering probability depends only on the angle between the incoming and outgoing directions, $\mu \equiv \cos\theta = \boldsymbol{n}\cdot\boldsymbol{n}'$. Therefore, with an appropriate choice of a scattering phase function $p(\mu)$ normalized such that $\int_{-1}^{1} p(\mu)\,\mathrm{d}\mu = 1$, we define the outgoing angular-averaged redistribution function as $R_{x'\to x} \equiv (4\pi)^{-2}\iint \mathrm{d}\Omega'\mathrm{d}\Omega R_{x',\boldsymbol{n}'\to x,\boldsymbol{n}} = \int_{-1}^{1} p(\mu) R_{x'\to x,\mu}\,\mathrm{d}\mu$. Furthermore, the conservation of photons in Eq. (1) requires a normalization[1] for the redistribution function of $\int_{-\infty}^{\infty} R_{x'\to x}\,\mathrm{d}x' = 1$, in accordance with the previous interpretation as a probability distribution function. Finally, the conversion to dimensionless frequency introduces a constant multiplicative factor, e.g. specific intensity, $I_x = \Delta\nu_\mathrm{D} I_\nu$, and frequency redistribution, $R_{x'\to x} = (\Delta\nu_\mathrm{D})^2 R_{\nu'\to\nu}$. Further discussion of the behavior of the redistribution function is provided in Appendix A, but for now we summarize the most relevant properties of redistribution in the wings by the average drift back toward the core and the rms displacement

$$\langle\delta x\rangle \sim -\frac{1}{x} \qquad \text{and} \qquad \sqrt{\langle\delta x^2\rangle} \sim 1 \,. \tag{4}$$

[1] This convention differs from that of Hummer [10], but is similar to that of Dijkstra [6]. For reference, our angle-averaged definition is related as $R^\mathrm{us}_{x'\to x} = R^\mathrm{Hummer}_{x'\to x}/\phi_\mathrm{Voigt}(x')$.

To simplify further, we define the zeroth and first order angular moments of the radiation intensity as $J_x \equiv \frac{1}{4\pi}\int \mathrm{d}\Omega I_x$ and $\boldsymbol{H}_x \equiv \frac{1}{4\pi}\int \mathrm{d}\Omega I_x \boldsymbol{n}$. These quantities are related to the energy density and flux by $E_x = \frac{4\pi}{c} J_x$ and $\boldsymbol{F}_x = 4\pi \boldsymbol{H}_x$, respectively. The emissivity is discretized as creation of photon MC packets each characterized by a particular energy ε_k, position $\boldsymbol{r}_k$, frequency x_k, and emission time t_k, such that $j_x \approx \sum \varepsilon_k \delta(\boldsymbol{r}_k)\delta(x_k)\delta(t_k)/(4\pi)$, where the index k refers to an individual MC packet. Without loss of generality we temporarily omit the emissivity term. The angular-averaged form of Eq. (1) is the zeroth order moment equation:

$$\frac{1}{c}\frac{\partial J_x}{\partial t} + \boldsymbol{\nabla}\cdot\boldsymbol{H}_x = -k_x J_x + \int k_{x'} J_{x'} R_{x'\rightarrow x}\mathrm{d}x' \,. \tag{5}$$

In the diffusion limit we may apply Fick's law as a closure relation to the moment equations:[2]

$$\boldsymbol{H}_x \approx -\frac{\nabla J_x}{3k_x} \,, \tag{6}$$

where the factor of 3 arises from the number of dimensions. Likewise, in the wings we can take advantage of the Fokker-Planck approximation to rewrite the redistribution integral as [18]

$$-k_x J_x + \int k_{x'} J_{x'} R_{x'\rightarrow x}\mathrm{d}x' \approx \frac{\partial}{\partial x}\left(\frac{k_x}{2}\frac{\partial J_x}{\partial x}\right) \,, \tag{7}$$

which naturally transforms frequency redistribution into a localized diffusion process.[3] Thus, after incorporating Eqs. (6) and (7) we have

$$\frac{1}{c}\frac{\partial J_x}{\partial t} = \nabla\cdot\left(\frac{\nabla J_x}{3k_x}\right) + \frac{\partial}{\partial x}\left(\frac{k_x}{2}\frac{\partial J_x}{\partial x}\right) \,. \tag{8}$$

This form places diffusion in space and frequency on equal footing.

At this point, we make additional assumptions to obtain an analytic solution for a static, isothermal, optically thick slab. This implies spatial-frequency independence for the absorption coefficient, $k(z,x) = k(z)H(x)$. In steady-state we discard the time-derivative and add a constant luminosity source, i.e. $\iiint j_\nu \mathrm{d}z\mathrm{d}\nu\mathrm{d}\Omega = \mathcal{L}$ with the spatial, frequency, and angular dependence isolated as $\eta(z)$, $H(x)/\sqrt{\pi}$, and $1/(4\pi)$, respectively (all normalized to unity):

$$\frac{1}{k(z)}\frac{\partial}{\partial z}\left(\frac{1}{k(z)}\frac{\partial J}{\partial z}\right) + \frac{3}{2}H(x)\frac{\partial}{\partial x}\left(H(x)\frac{\partial J}{\partial x}\right) = -\frac{3\mathcal{L}}{4\pi}\frac{\eta(z)}{k(z)}\frac{H^2(x)}{\sqrt{\pi}} \,. \tag{9}$$

We then apply a change of variables with $\mathrm{d}x = \sqrt{3/2}H(x)\,\mathrm{d}\tilde{x}$, $\mathrm{d}z = \mathrm{d}\tilde{z}/k(z)$, and $J = \tilde{J}\mathcal{L}\sqrt{6}/(4\pi)$. Here, $\tilde{z}$ represents the cumulative optical depth at line center starting from the center of the slab. Now in terms of the overall width of the line, $H^2(x)$ is sharply peaked at $x = 0$, so we can replace it with a delta function. To preserve normalization, we note that $\int 3H^2\mathrm{d}\tilde{x} = \int 3H^2(\mathrm{d}\tilde{x}/\mathrm{d}x)\,\mathrm{d}x = \int \sqrt{6}H\,\mathrm{d}x = \sqrt{6\pi}$. This gives a final equation of

$$\frac{\partial^2 \tilde{J}}{\partial \tilde{z}^2} + \frac{\partial^2 \tilde{J}}{\partial \tilde{x}^2} = -\frac{\eta(\tilde{z})}{k(\tilde{z})}\delta(\tilde{x}) \,. \tag{10}$$

---

[2] Fick's law can be derived by taking the first order moment equation, i.e.

$$\frac{1}{c^2}\frac{\partial \boldsymbol{F}_\nu}{\partial t} + \boldsymbol{\nabla}\cdot\mathsf{P}_\nu = -\frac{k_\nu \boldsymbol{F}_\nu}{c} \,,$$

and assuming the Eddington approximation $\mathsf{P}_\nu = \frac{1}{3}E_\nu \mathsf{I}$ and that the flux changes slowly in time $\partial \boldsymbol{F}_\nu/\partial t \approx 0$.

[3] The form of Eq. (7) technically violates photon conservation, but the correction factor proposed by Rybicki & Dell'Antonio [18] with frequency derivatives of $\boldsymbol{n}\cdot\boldsymbol{H}_x$ may safely be ignored for nearly isotropic radiation fields. Furthermore, Eq. (7) does not account for detailed balance, atomic recoil, or stimulated scattering. However, these are unlikely to be significant for many of the applications that utilize this approximation [17].

In Appendix B, we derive a general solution for the emission from an optically thick slab. For a central point source, the following is accurate when $a\tau_0 \gtrsim 10^3$ [7, 8, 13]:

$$\frac{J(x)}{\int J(x)\mathrm{d}x} = \sqrt{\frac{\pi}{6}}\frac{x^2}{a\tau_0}\mathrm{sech}\left(\sqrt{\frac{\pi^3}{54}}\frac{x^3}{a\tau_0}\right) . \tag{11}$$

Eq. (11) is a symmetric, double-peaked profile with peaks located at $x_\mathrm{p} = \pm 1.0664\,(a\tau_0)^{1/3}$, which is derived by setting $\partial J/\partial x = 0$ to obtain the transcendental relation $\bar{x}\tanh\bar{x} = 2/3$ with $\bar{x} = \sqrt{\pi^3/54}\,x^3/a\tau_0$. This characteristic escape frequency can be derived with a back of the envelope calculation. Recall that the typical redistribution in the wings generates an average drift back toward the core of $\langle\delta x\rangle \sim -1/x$ and a RMS displacement of $\sqrt{\langle\delta x^2\rangle} \sim 1$ [15]. Therefore, a wing photon tends to return to the core after $N_\mathrm{scat,wing} \sim x^2$ scatterings. In the optically-thick regime, escape occurs after an excursion in the wing to a characteristic escape frequency determined by setting the RMS displacement to the slab size, i.e. $N_\mathrm{scat,wing}^{1/2}\lambda_\mathrm{mfp} \approx R$. Therefore, the escape frequency is approximately

$$x_\mathrm{esc} \approx \left(\frac{a\tau_0}{\sqrt{\pi}}\right)^{1/3} , \tag{12}$$

the optical depth at this frequency is $\tau_\mathrm{esc} \approx x_\mathrm{esc}$, the mean free path is $\lambda_\mathrm{mfp} \approx R/x_\mathrm{esc}$, and the trapping (or diffusion) time is $t_\mathrm{trap} \approx x_\mathrm{esc}t_\mathrm{light}$ [2]. However, the total number of scatterings including core photons with short mean free paths is higher and may be estimated from the cumulative escape probability via $N_\mathrm{scat} \sim P_\mathrm{esc}^{-1} \sim [2\int_{x_\mathrm{esc}}^{\infty}\mathrm{d}x\phi(x)/x^2]^{-1} \sim \tau_0$ [1]. Physical scattering dominates the computational time for Lyα MCRT codes, so we expect the runtime to scale as $t_\mathrm{MC} \propto \tau_0$. With a core-skipping acceleration scheme this is improved to $t_\mathrm{MC,cs} \propto x_\mathrm{esc}^2 \propto (a\tau_0)^{2/3}$. In the next sections we outline two MCRT-based methods designed to further our intuition about Lyα transport in optically-thick media.

III. CONTINUOUS TRANSPORT

For simplicity we will only consider the static, uniform slab setup and we describe our algorithm in terms of individual photon trajectories. We do not consider transport through multiple cells, which in general requires Doppler-shifting into the correct local comoving frame in case the density, temperature, or bulk velocity of the gas changes. We first initialize the photon position at the center $z = 0$ and frequency at line center $x = 0$. We then combine scattering and movement together until the photon escapes, i.e. $z > |Z|$. At each scattering event the photon changes frequency. If the photon is in the core ($|x| \lesssim 3$ then we assign the new frequency to be $x = \pm x_\mathrm{cs}$, which is a core-skipping technique that assumes the mean-free-path is zero for core photons. If the photon is in the wing then we approximate the change in frequency by the first two frequency moments of the redistribution function, i.e. the new frequency is drawn from a Gaussian distribution with mean $x - 1/x$ and standard deviation 1. Finally, the photon moves by considering the random direction and interaction distance. The directional cosine with respect to the z-axis is drawn uniformly in $\mu \in [-1, 1]$. The optical depth to the next scattering event is drawn from an exponential distribution as $\Delta\tau = -\log(\xi)$, based on the uniform random number $\xi \in [0, 1]$. Finally, ray tracing reduces to a trivial integration, such that the traversed optical depth is proportional to distance, which means that the change in slab position for wing photons is

$$\Delta z = \mu\frac{\Delta\tau}{k(x)} \approx -\mu\log(\xi)\frac{\sqrt{\pi}Z}{a\tau_0}x^2 . \tag{13}$$

If the photon remains within the slab then the loop continues with a fresh iteration of scattering and moving. This represents the most basic (functional) Lyα MCRT code and we provide the following Python code as a demonstration.

```
## Track a single photon to escape ##
def photon():
    z = 0.                      # Initialize each photon at the center of the slab
    x = 0.                      # Initialize at line center: x = (nu - nu0) / DnuD
    while np.abs(z) < zmax:
        ## Scatter: 'frequency redistribution'
        if np.abs(x) < x_cw:    # Core-skipping = Zero mean free path approximation
            x = x_cs
            if rand() < 0.5: x = -x # Force symmetry for core-skipping
        else: # Wing scattering approximated by <dx> = -1/x and <dx^2> = 1
            x += normal() - 1. / x
        ## Move: Photon z position changes by cos(theta) * dtau / (k0 * H(x))
        mu = 2.*rand() - 1.     # Random direction: uniformly distributed in [-1,1]
        dtau = -np.log(rand()) # Random optical depth: dtau = -ln(R)
        z += mu * dtau * dz0 * x * x # i.e. dz = mu dtau / (k0 * H(x))
    return x
```

IV. DISCRETE DIFFUSION

The second method MCRT-based method is based on a discretized version of Eq. (8) rather than the continuous version from Eq. (1). A finite-volume discretization in space and frequency transforms the diffusion terms into source and sink terms dictating the movement of photon packets through cell boundaries and frequency bins. This process is quantitatively described by 'leakage coefficients'. We define the cell- and bin-averaged intensity by $J_{i,j} \equiv (\Delta V_i \Delta x_j)^{-1} \iint_{i,j} J_x \, \mathrm{d}V \mathrm{d}x$, with $\Delta V_i \equiv \int_i \mathrm{d}V$ denoting the volume of cell i, and $\Delta x_j \equiv \int_j \mathrm{d}x$ the width of frequency bin j. The spatial diffusion term becomes

$$\nabla \cdot \left(\frac{\nabla J_x}{3k_x} \right) \longrightarrow \sum_{\delta i} k^{\delta i}_{z\text{-leak}} (J_{\delta i,j} - J_{i,j}) \,, \tag{14}$$

where the summation is over all neighboring cells δi, the cells sharing a face with cell i. This discretization of the diffusion operator is based on a piecewise linear reconstruction with inflections at cell centers and interfaces. In the Monte Carlo interpretation the right hand side of Eq. (14) provides the mechanism for spatial transport. Likewise, the frequency diffusion term is

$$\frac{\partial}{\partial x} \left(\frac{k_x}{2} \frac{\partial J_x}{\partial x} \right) \longrightarrow \sum_{\delta j} k^{\delta j}_{x\text{-leak}} (J_{i,\delta j} - J_{i,j}) \,, \tag{15}$$

where the summation is over neighboring frequency bins δj. In the Monte Carlo picture the exchange on the right hand side of Eq. (15) provides the mechanism for frequency redistribution.

Substituting Eqs. (14) and (15) into Eq. (8) yields the fundamental equation for the resonant discrete diffusion Monte Carlo (rDDMC) scheme for resonant line transfer with a symmetric treatment of diffusion in both space and frequency [20]:

$$\frac{1}{c} \frac{\partial J_{i,j}}{\partial t} = \sum_{\delta i} k^{\delta i}_{z\text{-leak}} (J_{\delta i,j} - J_{i,j}) + \sum_{\delta j} k^{\delta j}_{x\text{-leak}} (J_{i,\delta j} - J_{i,j}) \,. \tag{16}$$

Eq. (16) is arranged to highlight photon flux conservation across cell/bin interfaces. The relative magnitudes of the leakage coefficients express the likelihood of the respective diffusion events.

The exact form for the leakage coefficients is determined by the specific geometry and discretization scheme. For concreteness, the general leakage coefficients for non-uniform Cartesian coordinates with Δz_i denoting the cell width in the leakage direction, and Δx_j denoting the frequency bin width (see [5] for a derivation; we also give the mean-free-paths for an isothermal, uniform medium with uniform spatial and frequency meshes):

$$k^{\delta i}_{z\text{-leak}} = \frac{1}{3\Delta z_i}\frac{2}{k_{i,j}\Delta z_i + k_{\delta i,j}\Delta z_{\delta i}} \qquad \Rightarrow \qquad \lambda^{\delta i}_{z\text{-leak}} = 3k_j(\Delta z)^2 \tag{17}$$

and

$$k^{\delta j}_{x\text{-leak}} = \frac{1}{\Delta x_j}\frac{1}{k^{-1}_{i,j}\Delta x_j + k^{-1}_{i,\delta j}\Delta x_{\delta j}} \qquad \Rightarrow \qquad \lambda^{\delta j}_{x\text{-leak}} = \left(k_j^{-1} + k_{\delta j}^{-1}\right)(\Delta x)^2 \,. \tag{18}$$

Here, the cell- and bin-averaged coefficients are defined by $k_{i,j} \equiv (\Delta V_i \Delta x_j)^{-1} \iint_{i,j} k_x \,\mathrm{d}V\mathrm{d}x$. We note that other discretizations or weighting kernels are possible but for simplicity we employ a tophat filter to simulate a piecewise constant frequency representation. Specifically, the Lyα absorption coefficient is $k_x = k_0\, H(a,x)$, where k_0 denotes the value at line center and the Hjerting–Voigt function is defined in Eq. (3) with a second order expansion in a of [see 19]

$$H(a,x) \approx e^{-x^2} + \frac{2a}{\sqrt{\pi}}\big(2x\,F(x) - 1\big) + a^2 e^{-x^2}\big(1 - 2x^2\big)\,, \tag{19}$$

where the Dawson integral is $F(x) = \int_0^x e^{y^2-x^2}\mathrm{d}y$. Integrating Eq. (19) over frequency yields

$$\mathcal{H}(a,x) \equiv \int_0^x H(a,y)\,\mathrm{d}y \approx \frac{\sqrt{\pi}}{2}\mathrm{erf}(x) - \frac{2a}{\sqrt{\pi}}F(x) + a^2\, x\, e^{-x^2}\,, \tag{20}$$

where the error function is $\mathrm{erf}(x) \equiv 2\int_0^x e^{-y^2}\mathrm{d}y/\sqrt{\pi}$. Thus, the mean absorption coefficient is

$$k_j = k_0\big(\mathcal{H}(a, x_j + \Delta x_j/2) - \mathcal{H}(a, x_j - \Delta x_j/2)\big)/\Delta x_j\,, \tag{21}$$

where for clarity we have dropped the spatial index and introduced the frequency bin center and width as x_j and Δx_j, respectively.

The Lyα rDDMC procedures used to solve Eq. (16) are similar to the continuous implementation of MCRT [see e.g. 6]. However, instead of following continuous photon trajectories, the DDMC packets are tracked by the cell index and frequency bin. When precise positions and frequencies are needed they can be drawn uniformly from the cell volume or bin interval. After a DDMC packet is initialized, leakage proceeds according to the smallest interaction distance:

$$\Delta\ell = \min_{\delta i,\delta j}\left(\Delta\ell^{\delta i}_{z\text{-leak}}, \Delta\ell^{\delta j}_{x\text{-leak}}\right)\,, \tag{22}$$

is executed to transport the photon packet across the appropriate cell or frequency bin interface. Here, the indices δi and δj run over all neighboring cells and frequency bins. The respective lengths are determined by drawing the effective optical depths from exponential distributions, such that

$$\Delta\ell_X = -\log(\xi)/k_X \qquad \text{for} \quad k_X \in \left\{k^{\delta i}_{z\text{-leak}}, k^{\delta j}_{x\text{-leak}}\right\}\,, \tag{23}$$

where ξ is a random number uniformly distributed in $[0,1]$, and the label X specifies the transport process. The result is shown in Fig. 1, which exactly matches the analytic solution from Eq. (11).

```
lambda_z = 3. * k * dz**2       # Mean free path for spatial leakage
k_inv = np.hstack([np.inf, 1./k[1:] + 1./k[:-1], np.inf])
lambda_x_L = k_inv[:-1] * dx**2 # Mean free path for frequency leakage (left)
lambda_x_R = k_inv[1:] * dx**2  # Mean free path for frequency leakage (right)

## Track a single photon to escape ##
def photon():
    iz = iz0                    # Initialize each photon at the center of the slab
    ix = ix0                    # Initialize at line center: x = (nu - nu0) / DnuD
    while True:
        dl_min = np.inf
        ## Check spatial leakage (left)
        dl_z_L = -np.log(rand()) * lambda_z[ix] # dl = -ln(R) / k_leak
        if dl_z_L < dl_min:
            action = MOVE_LEFT
            dl_min = dl_z_L
        ## Check spatial leakage (right)
        dl_z_R = -np.log(rand()) * lambda_z[ix] # dl = -ln(R) / k_leak
        if dl_z_R < dl_min:
            action = MOVE_RIGHT
            dl_min = dl_z_R
        ## Check frequency leakage (left)
        dl_x_L = -np.log(rand()) * lambda_x_L[ix] # dl = -ln(R) / k_leak
        if dl_x_L < dl_min:
            action = FREQ_LEFT
            dl_min = dl_x_L
        ## Check frequency leakage (right)
        dl_x_R = -np.log(rand()) * lambda_x_R[ix] # dl = -ln(R) / k_leak
        if dl_x_R < dl_min:
            action = FREQ_RIGHT
            dl_min = dl_x_R
        ## Update photon position (cell) or frequency (bin)
        if action == MOVE_LEFT:
            iz -= 1
            if iz < 0:
                break # Photon escapes through left boundary
        elif action == MOVE_RIGHT:
            iz += 1
            if iz >= nz:
                break # Photon escapes through right boundary
        elif action == FREQ_LEFT:
            ix -= 1
        elif action == FREQ_RIGHT:
            ix += 1
    return x[ix]
```

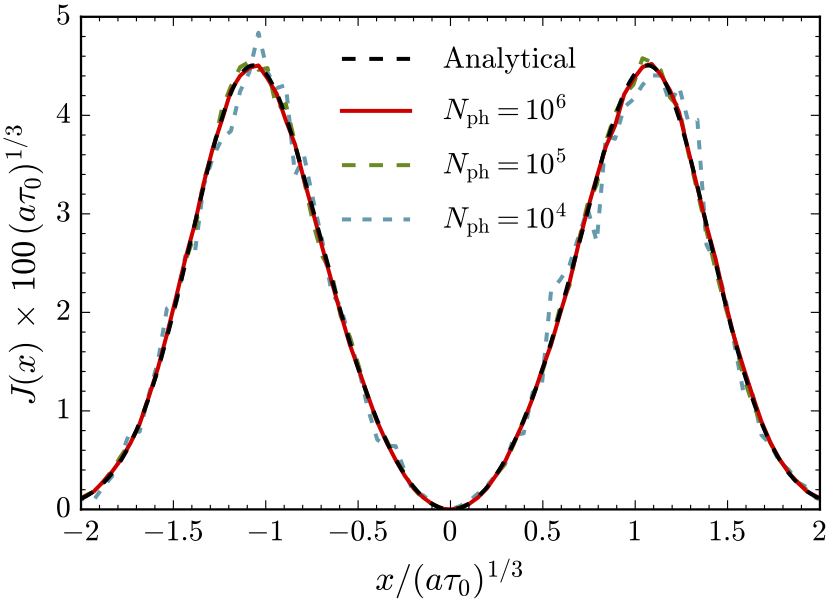

FIG. 1. Angular-averaged flux $J(x)$ for a homogeneous, static slab as a function of frequency. The axes have been rescaled by factors of $(a\tau_0)^{1/3}$ to remove the dependence on temperature and optical depth from the analytic solution. The simulations were run with $a\tau_0 = 10^9$ and $T = 10\,\mathrm{K}$. With a uniform resolution of $\Delta z \approx 0.01\,Z$ and $\Delta x \approx 0.05\,(a\tau_0)^{1/3}$, the Monte Carlo noise is still apparent when the number of photon packets is $N_{\rm ph} \approx 10^4$. Convergence is obtained by increasing $N_{\rm ph}$, yielding nearly exact agreement to the analytic solution with $N_{\rm ph} \approx 10^6$.

Appendix A: Approximations of the redistribution function

We now provide specific forms for the Lyα redistribution function. In particular, under isotropic coherent scattering without recoil, the redistribution function for the Voigt profile is [10, 21]

$$R_{\text{II-A}}(x,x') = \frac{1}{\pi H(x',a)} \int_\zeta^\infty e^{-u^2} \left[\tan^{-1}\left(\frac{\underline{x}+u}{a}\right) - \tan^{-1}\left(\frac{\bar{x}-u}{a}\right)\right] \mathrm{d}u\,, \tag{A1}$$

where $\bar{x} = \max(x,x')$, $\underline{x} = \min(x,x')$, and $\zeta = (\bar{x}-\underline{x})/2 = |x-x'|/2$. The limit as $a \to 0$ corresponds to the case with only Doppler broadening, so we may approximate the redistribution function in the core by

$$R_{\text{II-A,core}}(x,x') \approx R_{\text{I-A}}(x,x') = \frac{\sqrt{\pi}}{2} e^{x'^2} \mathrm{erfc}|\bar{x}|\,, \tag{A2}$$

where $|\bar{x}| = \max(|x|,|x'|)$. In this approximation core photons have an equal probability of being scattered in the range $|x| < |x'|$ with an exponentially decreasing probability of being scattered to other frequencies. On the other hand, in the limit of large frequencies $|x+x'| \to \infty$ the approximate redistribution function in the wing is

$$R_{\text{II-A,wing}}(x,x') \approx \left(\frac{2x'}{x+x'}\right)^2 \left[\frac{e^{-\zeta^2}}{\sqrt{\pi}} - \zeta\,\mathrm{erfc}(\zeta)\right]. \tag{A3}$$

The angular-averaged redistribution function under dipole scattering is qualitatively similar albeit with additional asymmetry because photons are preferentially forward- and back-scattered. We can gain some insight by considering the highest order frequency moments of the redistribution

function in the wings. Specifically, we calculate the frequency change ($\delta x \equiv x - x'$) moment of the portion in square brackets as

$$[\delta x^n] = \int_{-\infty}^{0} \delta x^n \left[\frac{e^{-\delta x^2/4}}{\sqrt{\pi}} + \frac{\delta x}{2}\,\mathrm{erfc}(-\delta x/2)\right] \mathrm{d}\delta x + \int_{0}^{\infty} \delta x^n \left[\frac{e^{-\delta x^2/4}}{\sqrt{\pi}} - \frac{\delta x}{2}\,\mathrm{erfc}(\delta x)\right] \mathrm{d}\delta x$$
$$= \frac{((-2)^n + 2^n)}{\sqrt{\pi}(n+2)}\Gamma\left(\frac{n+1}{2}\right) = \frac{4^m \Gamma\left(m+\frac{1}{2}\right)}{\sqrt{\pi}(m+1)} \qquad (\text{where } m = n/2)\,. \tag{A4}$$

Here only the even moments survive and the odd moments vanish. Therefore, we may expand the first term and integrate each term individually:

$$\langle \delta x^n \rangle \equiv \int_{-\infty}^{\infty} \delta x^n R_{\text{II-A,wing}}(\delta x, x')\mathrm{d}\delta x$$
$$= \sum_{k=0}^{\infty} \frac{(-1)^k (k+1)}{2^k x'^k} \left[\delta x^{n+k}\right]\,. \tag{A5}$$

If n is odd then only the odd k terms survive, and similarly if n is even then k must be even. Therefore, we consider the two cases separately:

$$\langle \delta x^{2m+1} \rangle = -\sum_{l=0}^{\infty} \frac{(l+1)}{4^l x'^{2l+1}} \left[\delta x^{2(m+l+1)}\right] \approx -\frac{1}{x'} \left[\delta x^{2(m+1)}\right] \approx -\frac{4^{m+1}\Gamma\left(m+\frac{3}{2}\right)}{\sqrt{\pi}(m+2)x'} \tag{A6}$$

$$\langle \delta x^{2m} \rangle = \sum_{l=0}^{\infty} \frac{(2l+1)}{4^l x'^{2l}} \left[\delta x^{2(m+l)}\right] \approx \left[\delta x^{2m}\right] \approx \frac{4^m \Gamma\left(m+\frac{1}{2}\right)}{\sqrt{\pi}(m+1)}\,. \tag{A7}$$

which leads to the desired result that the first two moments are $\langle \delta x \rangle \sim -1/x$ and $\langle \delta x^2 \rangle \sim 1$.

Appendix B: Analytic solution for an optically thick slab

We can find a general solution to Eq. (10) if the optical depth is finite. For simplicity we further assume the functions $\eta(z)$ and $k(z)$ are symmetric (even) about the central plane $z = 0$. Therefore, $\tilde{z} \in [-\tau_0, \tau_0]$ and the boundary conditions can be written as

$$\left(\frac{\partial \tilde{J}}{\partial \tilde{z}}\right)_{\tilde{z}=\tau_0} = fH(\tilde{x})\tilde{J}|_{\tilde{z}=\tau_0} \qquad \text{and} \qquad \lim_{\tilde{x}\to\pm\infty} \tilde{J} = 0\,. \tag{B1}$$

The domain of $\tilde{z}$ is compact so we employ an eigenfunction expansion with separable space and frequency so

$$\tilde{J}(\tilde{z}, \tilde{x}) = \sum_{n=1}^{\infty} \vartheta_n(\tilde{z})\varphi_n(\tilde{x})\,. \tag{B2}$$

The solutions of the homogeneous equation

$$\frac{\mathrm{d}^2 \vartheta_n}{\mathrm{d}\tilde{z}^2} + \lambda_n^2 \vartheta_n = 0\,, \tag{B3}$$

are of the form

$$\vartheta_n = N_n^{-1} \cos(\lambda_n \tilde{z}) \qquad \text{where} \quad n = 1, 2, \ldots\,, \tag{B4}$$

where the boundary conditions require the eigenvalues to satisfy the equation

$$\lambda_n \tan(\lambda_n \tau_0) = fH(\tilde{x})\,. \tag{B5}$$

Now if the optical depth is large out to any frequency with appreciable radiation, so photons escape before they diffuse to frequencies where the whole slab is optically thin, then it follows that

$$\lambda_n \tau_0 = \pi(n-1) + \tan^{-1}\left(\frac{fH(\tilde{x})}{\lambda_n}\right) \approx \pi\left(n - \frac{1}{2}\right) + \mathcal{O}\left(\frac{\pi n}{f\tau(\tilde{x})}\right)\,, \tag{B6}$$

where $\tau(\tilde{x}) \equiv \tau_0 H(\tilde{x})$. The normalization of orthogonal eigenfunctions is

$$N_n^2 = \int_{-\tau_0}^{\tau_0} \cos^2(\lambda \tilde{z})\,\mathrm{d}\tilde{z} = \tau_0 + \frac{\sin(2\lambda_n \tau_0)}{2\lambda_n \tau_0} \approx \tau_0\,. \tag{B7}$$

Upon substitution of Eq. (B2) into Eq. (10), multiplying by ϑ_m and integrating over $\tilde{z}$ we obtain

$$\frac{\mathrm{d}^2\varphi_n}{\mathrm{d}\tilde{x}^2} - \lambda_n^2 \varphi_n = -\frac{Q_n}{\sqrt{\tau_0}}\delta(\tilde{x})\,, \tag{B8}$$

where

$$Q_n = \int_{-\tau_0}^{\tau_0} \frac{\eta(\tilde{z})}{k(\tilde{z})}\cos(\lambda_n \tilde{z})\,\mathrm{d}\tilde{z} = 2\int_0^\infty \eta(z)\cos\left(\lambda_n \int_0^z k(z')\mathrm{d}z'\right)\,\mathrm{d}z\,. \tag{B9}$$

Away from $\tilde{x} = 0$, the solution satisfying the boundary conditions $\lim_{\tilde{x}\to\pm\infty}\tilde{J} = 0$, and the jump condition $\Delta(\mathrm{d}\varphi_n/\mathrm{d}\tilde{x})_{\tilde{x}=0} = -Q_n/\sqrt{\tau_0}$ derived from integrating Eq. (B8) is

$$\varphi_n = \frac{Q_n}{2\lambda_n\sqrt{\tau_0}} e^{-\lambda_n|\tilde{x}|}\,. \tag{B10}$$

Putting this all together we have a final solution of

$$\tilde{J}(\tilde{z},\tilde{x}) = \sum_{n=1}^{\infty} \frac{Q_n}{2\lambda_n\tau_0} e^{-\lambda_n|\tilde{x}|}\cos(\lambda_n\tilde{z})\,. \tag{B11}$$

The spectral line profile at the boundary is relevant for observations. We use Eq. (B5) to substitute $\cos(\lambda_n\tau_0) = \lambda_n \sin(\lambda_n\tau_0)/[fH(\tilde{x})] \approx \lambda_n \sin(\lambda_n\tau_0)/[fH(\tilde{x})] \approx \lambda_n(-1)^{n-1}/[fH(\tilde{x})]$, yielding

$$\tilde{J}(\tilde{x}) = \frac{e^{\pi|\tilde{x}|/2}}{2f\tau(\tilde{x})}\sum_{n=1}^{\infty}(-1)^{n-1}Q_n e^{-n\pi|\tilde{x}|}\,. \tag{B12}$$

To make further progress, we must consider specific cases for Q_n. For a central delta function source $\eta(z) = \delta(z)$ so $Q_n = 1$. We take advantage of the geometric series relation $\sum_{n=1}^{\infty} r^n = r/(1-r)$, or more specifically including minus signs $\sum_{n=1}^{\infty}(-1)^{n-1}r^n = r/(1+r)$, to simplify the expression to

$$\tilde{J}(\tilde{x}) = \frac{\mathrm{sech}(\pi|\tilde{x}|/2)}{4f\tau(\tilde{x})}\,. \qquad \text{(point source)} \tag{B13}$$

If the emissivity traces the absorption coefficient then $k(z) = 2\tau_0\eta(z)$. Therefore, the unknown constant from Eq. (B9) is

$$\begin{aligned} Q_n &= \int_0^\infty 2\eta(z)\cos\left(\lambda_n\tau_0\int_0^z 2\eta(z')\mathrm{d}z'\right)\,\mathrm{d}z \\ &= \int_0^1 \cos\left(\lambda_n\tau_0\zeta\right)\,\mathrm{d}\zeta = \frac{\sin(\lambda_n\tau_0)}{\lambda_n\tau_0} \approx \frac{(-1)^{n-1}}{\lambda_n\tau_0}\,, \end{aligned} \tag{B14}$$

and the expression for the spectral line profile from Eq. (B12) simplifies to

$$\tilde{J}(\tilde{x}) = \frac{1}{\pi f \tau(\tilde{x})} \tanh^{-1}\left(e^{-\pi|\tilde{x}|/2}\right) . \qquad \text{(uniform source, } \eta \propto k\text{)} \tag{B15}$$

---

[1] Adams T. F., 1972, ApJ, 174, 439
[2] Adams T. F., 1975, ApJ, 201, 350
[3] Ahn S.-H., Lee H.-W., Lee H. M., 2002, ApJ, 567, 922
[4] Auer L. H., 1968, ApJ, 153, 783
[5] Densmore J. D., Urbatsch T. J., Evans T. M., Buksas M. W., 2007, J. Comput. Phys., 222, 485
[6] Dijkstra M., 2014, Publ. Astron. Soc. Australia, 31, e040
[7] Dijkstra M., Haiman Z., Spaans M., 2006, ApJ, 649, 14
[8] Harrington J. P., 1973, MNRAS, 162, 43
[9] Henyey L. G., 1940, Proc. Natl. Acad. Sci., 26, 50
[10] Hummer D. G., 1962, MNRAS, 125, 21
[11] Lee J.-S., 1974, ApJ, 192, 465
[12] Loeb A., Rybicki G. B., 1999, ApJ, 524, 527
[13] Neufeld D. A., 1990, ApJ, 350, 216
[14] Neufeld D. A., 1991, ApJ, 370, L85
[15] Osterbrock D. E., 1962, ApJ, 135, 195
[16] Partridge R. B., Peebles P. J. E., 1967, ApJ, 147, 868
[17] Rybicki G. B., 2006, ApJ, 647, 709
[18] Rybicki G. B., Dell'Antonio I. P., 1994, ApJ, 427, 603
[19] Smith A., Safranek-Shrader C., Bromm V., Milosavljević M., 2015, MNRAS, 449, 4336
[20] Smith A., Tsang B. T. H., Bromm V., Milosavljević M., 2018, MNRAS, 479, 2065
[21] Unno W., 1952, PASJ, 4, 100
[22] Zanstra H., 1949, Bull. Astron. Inst. Netherlands, 11, 1
[23] Zheng Z., Miralda-Escudé J., 2002, ApJ, 578, 33